Supplementary material for the manuscript entitled "Use of ssq rotational invariant of magnetotelluric impedances for estimating informative properties for galvanic distortion"

Rung-Arunwan T.[1,2,3,*], Siripunvaraporn W.[1,2] and Utada H.[3]

[1] Department of Physics, Faculty of Science, Mahidol University, 272 Rama 6 Road, Rachatawee, Bangkok 10400, THAILAND

[2] Thailand Center of Excellence in Physics, Commission on Higher Education, 328 Si Ayutthaya Road, Bangkok 10400, THAILAND

[3] Earthquake Research Institute, University of Tokyo, Yayoi 1-1-1, Bunkyo-ku, Tokyo, 113-0032 JAPAN

[*] Now at Curl-E Geophysics Co., Ltd., Bangkok, THAILAND

t.rungarunwan@gmail.com

wsiripun@gmail.com

utada@eri.u-tokyo.ac.jp

Preprint submitted to *Earth Planets Space* on May 24, 2017

Abstract

In the manuscript, we proposed the estimation of the regional mean one-dimensional (1D) conductivity profile with the average ssq impedance instead of using the traditional Berdichevsky average and detecting the galvanic distortion in MT data with the det and ssq impedances. The theoretical formulation of the proposed methods is based on the Groom–Bailey model of galvanic distortion. Therefore, the galvanic distortion model dependence of the proposed methods is questionable. The first section of this supplementary material compares the geometric average, which is a basis of the proposed methods, to the arithmetic average. The geometric and arithmetic averages of the det and ssq impedances from the synthetically distorted data are calculated. For different distortion models, the geometric average of ssq impedances is shown to be the most reliable in estimating the regional mean 1D conductivity profile. The second section of this supplement shows the numerical results supporting the approximation applied in averaging the distorted ssq impedances. The third section shows the examples of all four elements of the impedance tensors, undistorted and distorted, from all stations in our three-dimensional (3D) example. The last section provides the theoretical derivation and numerical examination of the proposed methods using the other model of galvanic distortion. Therefore, the perturbation of the identity matrix, which is referred to as the PIM model. The numerical results shown that the models of galvanic distortion insignificantly affect the conclusion in the manuscript, i.e., the average ssq impedance is the appropriate choice for estimating a regional mean 1D conductivity profile.

Keywords

Magnetotellurics–Rotational invariant–Galvanic distortion

1. Geometric and arithmetic means of distorted impedances

Both geometric and arithmetic averages are used for measuring the central tendency of random variables. Mathematically, the arithmetic mean is greater than or equal to the geometric mean for non-negative numbers. The geometric mean is known to be less sensitive to the outliers compared to the arithmetic mean (Dawson and Trapp 2004). As a consequence, the arithmetic mean may not be appropriate in case of random variables with skewed distribution. The magnitude of MT data, the apparent resistivity, is shown in a logarithmic scale. The regional mean impedance was originally calculated using the geometric average (Berdichevsky et al. 1980), upon which the proposed method is based (Rung-Arunwan et al. 2016). However, either the geometric mean (e.g., Berdichevsky et al. 1980; Avdeeva et al. 2015) or the arithmetic mean (e.g., Baba et al. 2010) has been used to determine the regional mean rotationally-invariant impedances. The dependence of the regional mean rotationally-invariant impedances on averaging approaches has never been investigated. In the following, we examined the geometric and arithmetic means for the synthetically distorted data from both the parametric and numerical models.

The arithmetic means of the det and ssq impedances in one-dimensional (1D) Earth, $\bar{Z}'_{\mathrm{det,A}}(\omega)$ and $\bar{Z}'_{\mathrm{ssq,A}}(\omega)$, are written as follows:

$$\bar{Z}'_{\mathrm{det,A}}(\omega) = \frac{1}{N}\sum_{i=1}^{N} Z'_{\mathrm{det}}(\mathbf{r}_i;\omega) \tag{S1}$$

and

$$\bar{Z}'_{\mathrm{ssq,A}}(\omega) = \frac{1}{N}\sum_{i=1}^{N} Z'_{\mathrm{ssq}}(\mathbf{r}_i;\omega), \tag{S2}$$

where the definitions of variables are given in the main text.

The examples of the geometric and arithmetic average of the det and ssq impedances distorted under the Groom–Bailey and PIM models (see Section 4 of this supplementary material) are shown in Figures S1a and S2a. The arithmetic averages of both det and ssq impedances are greater than the geometric averages of those for both galvanic distortion models, which is consistent with the theoretical prediction. Consequently, the average det impedance gives the regional mean 1D impedance comparable to the average ssq impedance and also to the undistorted impedance.

The 1D models inverted from these average responses are inverted with the same condition as in the main text (They are shown in Figures S1b, and S2b). For the parametric models of galvanic distortion, the arithmetic-average det impedance and the geometric-average ssq impedance give the 1D models that

Galvanic distortion model	Geometric average		Arithmetic average	
	ssq	det	ssq	det
Groom–Bailey model (SD=0.3)	0.0027	0.1954	0.3453	0.0530
PIM model (SD=0.5)	0.0874	0.2411	0.1985	0.1045

Table S1. : Model recovery misfits (Eq. S3) calculated from the 1D models estimated from the distorted data relative to the 1D model estimated from the undistorted data (Figures S1b, and S2b) within the depth range of 14.8–33.3 km.

are consistent with the 1D model inverted from the undistorted data. However, to quantitatively validate such averages, we used the model recovery misfit (after Zhang et al. 2012), which is the RMS misfit of the conductivity model parameters estimated from distorted data with respect to those from undistorted data:

$$\mathrm{rms}(\sigma) = \sqrt{\frac{\sum_{i=1}^{L}(\log\sigma_{\mathrm{d},i} - \log\sigma_{\mathrm{u},i})^2}{L}}, \tag{S3}$$

where $\log\sigma_{\mathrm{d},i}$ and $\log\sigma_{\mathrm{u},i}$ are estimated conductivity at the ith layer from the distorted and undistorted data, respectively, and L is the number of selected layers. Here, only the model parameters within the depth range of 14.8–33.3 km, which corresponds to the periods of present interest, are used in calculation. The model recovery misfits of the synthetically distorted data are given in Table S1. The models from the geometric-average ssq impedances give the least model recovery misfits, while the model recovery misfit from the geometric-average ssq impedance and that from the arithmetic-average det impedance are equivalent. Although, the arithmetic-average det impeance and the geometric-average ssq impedance may be comparable in some cases, the quantitative validation supports the use of the geometric average which is a basis of the proposed methods.

2. The contribution of the structural dimensionality to the distorted ssq impedance

An expression of the ssq rotational invariant of the distorted impedance observed at the ith station as shown in Rung-Arunwan et al. (2016) in terms of the regional (undistorted) impedance and the distortion parameters is written as

$$\begin{aligned}\mathrm{ssq}(\mathbf{Z}'(\mathbf{r}_i;\omega)) &= Z'_{xx}(\mathbf{r}_i;\omega)^2 + Z'_{xy}(\mathbf{r}_i;\omega)^2 + Z'_{yx}(\mathbf{r}_i;\omega)^2 + Z'_{yy}(\mathbf{r}_i;\omega)^2 \\ &= g_i^2 \mathrm{ssq}(\mathbf{Z}_\mathrm{R}(\mathbf{r}_i;\omega)) \\ &\quad - \frac{2g_i^2\, s_i}{(1+s_i^2)}\left[Z^\mathrm{R}_{xx}(\mathbf{r}_i;\omega)^2 + Z^\mathrm{R}_{xy}(\mathbf{r}_i;\omega)^2 - Z^\mathrm{R}_{yx}(\mathbf{r}_i;\omega)^2 - Z^\mathrm{R}_{yy}(\mathbf{r}_i;\omega)^2\right] \\ &\quad + \frac{4g_i^2\, e_i(1-s_i^2)}{(1+e_i^2)(1+s_i^2)}\left[Z^\mathrm{R}_{xx}(\mathbf{r}_i;\omega)Z^\mathrm{R}_{yx}(\mathbf{r}_i;\omega) + Z^\mathrm{R}_{yx}(\mathbf{r}_i;\omega)Z^\mathrm{R}_{yy}(\mathbf{r}_i;\omega)\right],\end{aligned} \tag{S4}$$

where the $\mathbf{r}_i$ is the position vector of the ith station, the ω is the angular frequency, and the superscript (and subscript) R represents the regional or undistorted impedance. The first term is the ssq rotational invariant of the regional (scaled) impedance tensor. The second and third terms will, respectively, be finite if the underlying structure is two-dimensional (2D) or three-dimensional (3D) and the geometric distortion (splitting and shear) exists. Without geometric distortion, the second and third terms vanish regardless of structure dimensionality.

Rung-Arunwan et al. (2016) mentioned that the contributions from the second and third terms may be small compared to that from the first term, and the contributions from the second and third terms are minor after averaging over many MT stations (see Eq. 7). To clarify the claims, we define the contributions from the second and third terms to the distorted ssq rotational invariant (Eq. S4) as the ratios R_2 and R_3:

$$R_2(\mathbf{r}_i;\omega) = \left|\frac{-\frac{2g_i^2\, s_i}{(1+s_i^2)}\left[Z^\mathrm{R}_{xx}(\mathbf{r}_i;\omega)^2 + Z^\mathrm{R}_{xy}(\mathbf{r}_i;\omega)^2 - Z^\mathrm{R}_{yx}(\mathbf{r}_i;\omega)^2 - Z^\mathrm{R}_{yy}(\mathbf{r}_i;\omega)^2\right]}{\mathrm{ssq}(\mathbf{Z}'(\mathbf{r}_i;\omega))}\right|, \tag{S5}$$

and

$$R_3(\mathbf{r}_i;\omega) = \left|\frac{\frac{4g_i^2\, e_i(1-s_i^2)}{(1+e_i^2)(1+s_i^2)}\left[Z^\mathrm{R}_{xx}(\mathbf{r}_i;\omega)Z^\mathrm{R}_{yx}(\mathbf{r}_i;\omega) + Z^\mathrm{R}_{yx}(\mathbf{r}_i;\omega)Z^\mathrm{R}_{yy}(\mathbf{r}_i;\omega)\right]}{\mathrm{ssq}(\mathbf{Z}'(\mathbf{r}_i;\omega))}\right|. \tag{S6}$$

The example of the ratios R_2 and R_3 from the checkerboard model (Figure 8 in the main text) at the period of 316.2 s, where the distortion parameter with SD of 0.3 is applied, are shown in Figure S3. The variation in the magnitude of the ssq rotational invariant due to the underlying structure is significantly less than the fluctuation due to the galvanic distortion. This can be seen from the plot of the undistorted ssq rotational invariant (Figure S3a) compared to that of the distorted ssq rotational invariant (Figure S3b). The plots of the ratios R_2 and R_3 (Figures S3c and S3d) show that the contributions from the

second and third terms of Eq. S4 to the distorted ssq rotational invariants are minor (approximately less than 5%). This implies that the contribution from the first term of Eq. S4, i.e., the ssq rotational invariant of the regional (or undistorted) impedance with site gain, dominates those from the second and third terms and it is the major part of the distorted ssq rotational invariant.

To represent the case of the more 2D-like structure, the checkerboard is elongated in y direction (Figure S4). Note that the induction number of the elongated checkerboard is slightly larger than the square one. Here, only the example of ssq impedance is shown to avoid redundancy because the bias in the det impedances from the elongated checkerboard is similar to those from the square case. The MT responses from this setup are calculated and distorted with different SD of distortion parameters under the Groom–Bailey model, and the ssq impedances are calculated and then averaged (Figure S5a) using Eq. (7). The average impedances are inverted (Figure S5b) in the same manner as in the main text.

As with the square checkerboard case, the variation in the magnitude of the ssq rotational invariant due to the galvanic distortion is stronger than that from the underlying structure (Figures S6a and S6b). The ssq rotational invariant of the distorted impedance and the ratios R_2 and R_3 (Eqs. S5 and S6) from the elongated checkerboard model at the period of 316.2 s, where the distortion parameter with SD of 0.3 is applied, is shown in Figure S6. When the underlying structure is more 2D like, the contribution from the second term (Figure S6c) becomes stronger (compared to the square checkerboard model). However, the contributions from the second and third terms to the distorted ssq rotational invariants are still minor (Figures S6c and S6d). Only a few stations show 10–15% contribution to the distorted ssq rotational invariants.

To demonstrate that the contribution from the second and third terms are negligible in averaging the ssq impedances from a cluster of N MT stations, we define the ratio $\bar{R}_1$:

$$\bar{R}_1(\omega) = \left| \prod_{i=1}^{N} \frac{\mathrm{ssq}(\mathbf{Z}'(\mathbf{r}_i;\omega))}{g_i^2 \mathrm{ssq}(\mathbf{Z}_\mathrm{R}(\mathbf{r}_i;\omega))} \right|^{1/N} . \tag{S7}$$

This frequency-dependent ratio represents the contribution from the first term in the average ssq impedance. If the average ssq impedance is mostly contributed by the first term, the ratio $\bar{R}_1$ will approach unity. To demonstrate that using the larger number of MT observation will lead to the more reliable average impedance, we vary the number of MT stations and the array configuration as shown in Figure S7.

The ratio $\bar{R}_1$ calculated from the checkerboard model (Figure S8) is approximately unity. This

indicates that the average of the distorted ssq rotational invariant is merely equal to the average ssq rotational invariants of the regional impedance including the site gain and the contributions from the second and third terms should be negligible. Moreover, estimating the regional mean 1D conductivity profile would be more reliable as seen from the smaller standard error, if more of MT observations are made in the same size of the interesting area.

Therefore the claims that the contributions from the second and third terms are small and negligible after averaging over a number of MT observation are acceptable at least for the example shown in this paper.

3. MT impedances from 3D example

In this section, four components of MT impedances from the cluster in a 3D example (Figure 8) in the main text are presented. The diagonal components, xx and yy, are shown to be minor compared to the off-diagonal components, xy and yx (Figure S9), if no galvanic distortion is applied. Their magnitudes are a few decades smaller than those of the off-diagonal components. However, when the galvanic distortion is contained, the diagonal components become significant, particularly due to the geometric distortion (see Groom and Bailey 1989). Here, an example of 3D responses distorted with the distortion parameter with SD of 0.3 is chosen (Figure S10). The magnitudes of off-diagonal and diagonal components become comparable and the phase mixing is also observed.

4. Examining the PIM model of galvanic distortion

In MT, the distorted impedance tensor $\mathbf{Z}'$ is mathematically expressed as the product of the distortion operator $\mathbf{C}$ and the regional (or undistorted) impedance tensor $\mathbf{Z}_{\mathrm{R}}$:

$$\mathbf{Z}' = \mathbf{C}\mathbf{Z}_{\mathrm{R}}, \tag{S8}$$

where the distortion operator $\mathbf{C}$ is the 2×2 rank-2 tensor of real-valued numbers so four degrees of freedom are required (Smith 1995). This paper and also Rung-Arunwan et al. (2016) have adopted the Groom–Bailey model of galvanic distortion (Groom and Bailey 1989) to model the distortion operator. In this paper, we made synthetic tests by examining the behaviours of 'randomized distortion operators', which were generated by giving Gaussian random numbers to the controlling parameters of the Groom–Bailey model. Therefore, the site gain parameter follows the log-normal distribution with the mean of unity, which is consistent with the Berdichevsky's concept. However, the Groom–Bailey model is not the only way to parameterize the distortion operator. A number of models have been proposed, for example, by Bahr (1988), Chave and Smith (1994) and Smith (1995). In general, we may write the distortion operator $\mathbf{C}$ as a product of the site gain g and the tensor of geometric distortion $\tilde{\mathbf{C}}$:

$$\mathbf{C} = g\tilde{\mathbf{C}}. \tag{S9}$$

Here $\tilde{\mathbf{C}}$ is normalized so that its Frobenius norm is unity. For example, the geometric distortion tensors in the Groom–Bailey model—twist $\mathbf{T}$, shear $\mathbf{S}$, splitting $\mathbf{A}$ operators—are normalized by their Frobenius norms. Another model of galvanic distortion, the perturbed identity matrix (PIM) model, which is mostly adopted recently (e.g., Tietze et al. 2015) takes a form of perturbation of the identity matrix:

$$\begin{gathered}\mathbf{C} = \mathbf{I} + \mathbf{D} \\ \begin{bmatrix} C_{xx} & C_{xy} \\ C_{yx} & C_{yy} \end{bmatrix} = \begin{bmatrix} 1 & 0 \\ 0 & 1 \end{bmatrix} + \begin{bmatrix} D_{xx} & D_{xy} \\ D_{yx} & D_{yy} \end{bmatrix},\end{gathered} \tag{S10}$$

where $\mathbf{I}$ is the identity matrix, and $\mathbf{D}$ is the perturbation matrix, elements of which—D_{xx}, D_{xy}, D_{yx}, D_{yy}—describe the distortion. It is possible to synthesize a 'randomized distortion' by giving random number to D_{xx}, D_{xy}, D_{yx}, and D_{yy}. In analogy to Eq. (S9), the normalized geometric distortion tensor can be written as

$$\tilde{\mathbf{C}} = \frac{\mathbf{C}}{\|\mathbf{C}\|/\sqrt{2}}, \tag{S11}$$

where the $\|\mathbf{C}\| = \sqrt{C_{xx}^2 + C_{xy}^2 + C_{yx}^2 + C_{yy}^2}$ is the Frobenius norm of $\mathbf{C}$. Note that when the tensors are real-valued, the Frobenius norm squared and the ssq of those tensors are equivalent. In the PIM model,

the site gain (g in Eq. S9) can thus be defined from the Frobenius norm (Bibby et al. 2005):

$$g^{\mathrm{frb}} = \frac{\|\mathbf{C}\|}{\sqrt{2}}, \tag{S12}$$

which is hereafter named the Frobenius gain. Note that the site gain is not treated as an independent parameter in this galvanic distortion model. If the $(C_{xx}, C_{xy}, C_{yx}, C_{yy})$ cohorts follow the normal distribution, the $\|\mathbf{C}\|^2$ is a random variable following the χ^2 distribution of the fourth order. Therefore, the distribution of the Frobenius gain for the PIM model is expected to be non-Gaussian. The mean value is expected to be greater than unity.

Under the PIM model of galvanic distortion, the det and ssq impedances from the distorted 1D impedance tensor at the ith station can be, respectively, expressed as:

$$Z'_{\mathrm{det}}(\mathbf{r}_i;\omega) = \sqrt{\det(\mathbf{C}_i)}\, Z_{\mathrm{1D}}(\omega) = \sqrt{C_{xx,i}C_{yy,i} - C_{xy,i}C_{yx,i}}\, Z_{\mathrm{1D}}(\omega), \tag{S13}$$

and

$$Z'_{\mathrm{ssq}}(\mathbf{r}_i;\omega) = \frac{\|\mathbf{C}_i\|}{\sqrt{2}}\, Z_{\mathrm{1D}}(\omega) = \sqrt{(C^2_{xx,i} + C^2_{xy,i} + C^2_{yx,i} + C^2_{yy,i})/2}\, Z_{\mathrm{1D}}(\omega). \tag{S14}$$

Note that the coefficient of the distorted det impedance is generally smaller than that of the distorted ssq impedance because:

$$C_{xx,i}C_{yy,i} - C_{xy,i}C_{yx,i} \leq (C^2_{xx,i} + C^2_{xy,i} + C^2_{yx,i} + C^2_{yy,i})/2 \tag{S15}$$

Consequently, the det impedance is expected to give the smaller impedance magnitude.

From an array of N MT stations, the average det and ssq impedances are written as:

$$\bar{Z}'_{\mathrm{det}}(\omega) = \left[\prod_{i=1}^{N} \sqrt{\det(\mathbf{C}_i)}\right]^{\frac{1}{N}} Z_{\mathrm{1D}}(\omega) = \left[\prod_{i=1}^{N} C_{xx,i}C_{yy,i} - C_{xy,i}C_{yx,i}\right]^{\frac{1}{2N}} Z_{\mathrm{1D}}(\omega), \tag{S16}$$

$$\bar{Z}'_{\mathrm{ssq}}(\omega) = \left[\prod_{i=1}^{N} \frac{\|\mathbf{C}_i\|}{\sqrt{2}}\right]^{\frac{1}{N}} Z_{\mathrm{1D}}(\omega) = \left[\prod_{i=1}^{N} \frac{C^2_{xx,i} + C^2_{yy,i} + C^2_{xy,i} + C^2_{yx,i}}{2}\right]^{\frac{1}{2N}} Z_{\mathrm{1D}}(\omega). \tag{S17}$$

As the distortion tensor $\mathbf{C}$ in the PIM model is the perturbation of the identity matrix, the geometric average of $\|\mathbf{C}_i\|/2$ is slightly greater than unity if the distortion is strong. Therefore, the ssq impedance may give the underestimated regional mean 1D conductivity profile under the PIM model.

Moreover, we can derive the galvanic distortion indicators for the PIM model of galvanic distortion. With the definition in Eq. (8) in the main text, the local distortion indicator (LDI) for 1D case is

$$\gamma_i = \frac{(C^2_{xx,i} + C^2_{yy,i} + C^2_{xy,i} + C^2_{yx,i})/2}{C_{xx,i}C_{yy,i} - C_{xy,i}C_{yx,i}}. \tag{S18}$$

From the relationship in Eq. (S15), the LDI is expected to be greater than unity, if the galvanic distortion exists in the data. Furthermore, we can define the apparent gain in the PIM model. As with Eq. (11) in the manuscript,

$$g_i^{\mathrm{ssq}} = \frac{Z'_{\mathrm{ssq}}(\mathbf{r}_i;\omega)}{\bar{Z}'_{\mathrm{ssq}}(\omega)}. \tag{S19}$$

The apparent ssq gain is expected to be a good approximation of the Frobenius gain g_i^{frb} in cases of weak and moderate distortion. However, if the galvanic distortion is strong, the apparent ssq gain may underestimate the gain derived from the Frobenius norm.

To examine whether and how the proposed method depends on the choice of galvanic distortion model, we made a few tests with the synthetic data distorted under the PIM model of galvanic distortion in the similar manner with the example in Section 3 of the main text.

Each of four elements of $\mathbf{D}$ is assumed real-valued random number following the normal distribution with zero mean, and the 25 random $(D_{xx}, D_{xy}, D_{yx}, D_{yy})$ cohorts for 25 MT stations were then generated. We used five SD values—0.1, 0.2, 0.3, 0.4, and 0.5—to control the galvanic distortion strength (Figure S11a). Note that with this small number of samples the distribution of $(D_{xx}, D_{xy}, D_{yx}, D_{yy})$ cohorts is less likely to obey the normal distribution when the SD is large, i.e., greater than 0.3. Note that the Groom–Bailey parameterization produces the more significant perturbation at the same SD for the distortion parameter distribution (Figure S11b). At each galvanic distortion strength, the $(D_{xx}, D_{xy}, D_{yx}, D_{yy})$ cohorts are used to calculate the distortion operator using Eq. (S10) and then applied to the 1D synthetic data (Figure 2). The det and ssq impedances from the distorted impedance tensors were then averaged (Figure S12).

The models of the regional mean 1D conductivity profiles (Figure S13) were derived from inverting the average det and ssq impedances in the same manner (as in Section 3). From the results of applying the PIM model of galvanic distortion, the models of regional mean 1D profile from the average ssq impedance is shown to be slightly dependent upon the galvanic distortion model, while those from the average det impedance is shown to be biased toward more conductive and shallower side. As expected, the average ssq impedance slightly overestimates the regional mean 1D impedance, i.e., giving an underestimated conductivity profile under the PIM model depending on the SD value. This is partly because defining the distortion operator $\mathbf{C}$ as the perturbation of the identity matrix gives the geometric average of $\|\mathbf{C}_i\|$ over a large number of samples greater than unity. However, the effect is much smaller than the amount of bias in the distorted det impedances (Figures S13). The example of the LDIs from distorted data are

shown in Figure S14. As expected, the LDIs are greater than unity, if the data is distorted. As with using the Groom–Bailey model, the LDIs can point out the presence or absence of the galvanic distortion under the PIM model.

As with Eq. (16) in the main text, the mean apparent ssq gain of the ith station $\bar{g}_i^{\mathrm{ssq}}$ under the PIM model (Figure S15) is obtained, and it underestimates the Frobenius gain. This is because the average ssq impedance overestimates the regional mean 1D impedance, as described above. As predicted, the Frobenius gain and also the mean apparent ssq gain obey the χ^2 distribution (Figure S16). The percentage difference of the mean apparent ssq gain with respect to the Frobenius gain is calculated using

$$\mathcal{P}(\bar{g}_i^{\mathrm{ssq,frb}}) = \frac{\bar{g}_i^{\mathrm{ssq}} - g_i^{\mathrm{frb}}}{g_i^{\mathrm{frb}}} \times 100. \tag{S20}$$

The difference is only 6% in all cases.

Although the mean apparent ssq gain underestimates the Frobenius gain, the underestimation is only a few percent (about 6%) even in the case of severe distortion (SD=0.5). Therefore, the apparent ssq gain can still be a good approximation of the Frobenius gain.

References

Avdeeva A, Moorkamp M, Avdeev D, Jegen M, Miensopust M (2015) Three-dimensional inversion of magnetotelluric impedance tensor data and full distortion matrix. Geophysical Journal International 202(1):464–481

Baba K, Utada H, Goto TN, Kasaya T, Shimizu H, Tada N (2010) Electrical conductivity imaging of the Philippine Sea upper mantle using seafloor magnetotelluric data. Physics of the Earth and Planetary Interiors 183(1–2):44–62, Special Issue on Deep Slab and Mantle Dynamics

Bahr K (1988) Interpretation of the magnetotelluric impedance tensor: Regional induction and local telluric distortion. Journal of Geophysics 62:119–127

Berdichevsky M, Vanyan L, Kuznetsov V, Levadny V, Mandelbaum M, Nechaeva G, Okulessky B, Shilovsky P, Shpak I (1980) Geoelectrical model of the Baikal region. Physics of the Earth and Planetary Interiors 22(1):1–11

Bibby HM, Caldwell TG, Brown C (2005) Determinable and non-determinable parameters of galvanic distortion in magnetotellurics. Geophysical Journal International 163:915–930

Chave AD, Smith JT (1994) On the electric and magnetic galvanic distortion tensor decompositions. Journal of Geophysical Research 99(B3):4669–4682

Dawson B, Trapp RG (2004) Basic & clinical biostatistics. In: Basic & clinical biostatistics, Lange Medical Books; McGraw-Hill

Groom RW, Bailey RC (1989) Decomposition of magnetotelluric impedance tensors in the presence of local three-dimensional galvanic distortion. Journal of Geophysical Research: Solid Earth 94(B2):1913–1925

Rung-Arunwan T, Siripunvaraporn W, Utada H (2016) On the Berdichevsky average. Physics of the Earth and Planetary Interiors 253:1–4

Smith JT (1995) Understanding telluric distortion matrices. Geophysical Journal International 122:219–226

Tietze K, Ritter O, Egbert GD (2015) 3-D joint inversion of the magnetotelluric phase tensor and vertical magnetic transfer functions. Geophysical Journal International 203(2):1128–1148

Zhang L, Koyama T, Utada H, Yu P, Wang J (2012) A regularized three-dimensional magnetotelluric inversion with a minimum gradient support constraint. Geophysical Journal International 189(1):296–316

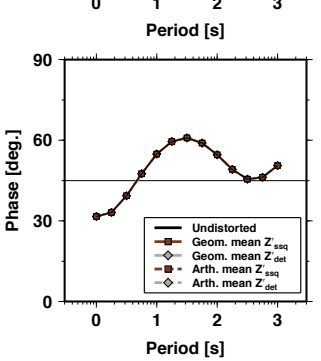

(a)

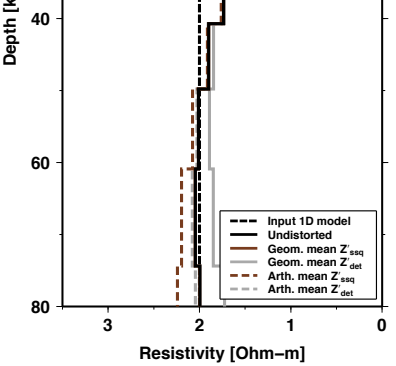

(b)

Figure S1. : (a) The geometric (symbols with solid lines) and arithmetic (symbols with dashed lines) averages of the det (gray diamonds) and ssq (brown squares) impedances from the data distorted with the Groom–Bailey model, where the distortion parameter cohorts with an SD of 0.3 was applied. These averages are shown in comparison with the undistorted response (black solid line). (b) The models estimated from the geometric (solid lines) and arithmetic (dashed lines) average det (gray) and ssq (brown) impedances. The estimated 1D models are compared with the input 1D model (black dashed line) and the 1D model estimated from the undistorted data (black solid line).

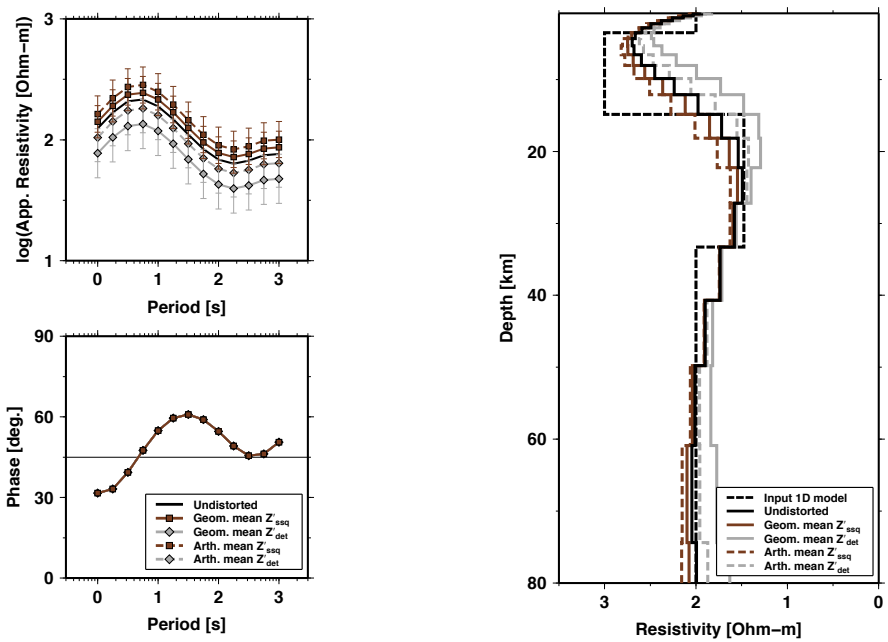

(a) (b)

Figure S2. : Same as Figure S1 for the PIM model where the $(D_{xx}, D_{xy}, D_{yx}, D_{yy})$ cohorts with an SD of 0.5 was applied.

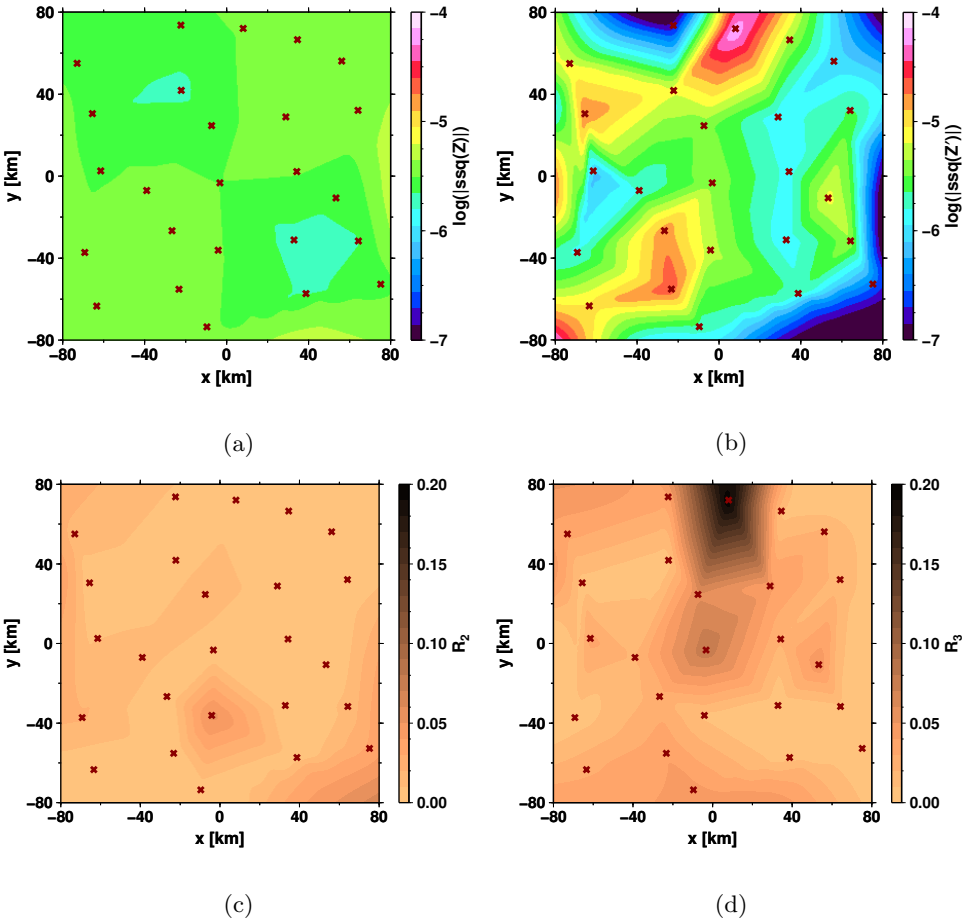

Figure S3. : Absolute values of the (a) undistorted and (b) distorted ssq rotational invariants, and the ratios R_2 and R_3 (Eqs. S5 and S6, respectively) at the period of 316.2 s calculated from the checkerboard model (Figure 8 in the main text).

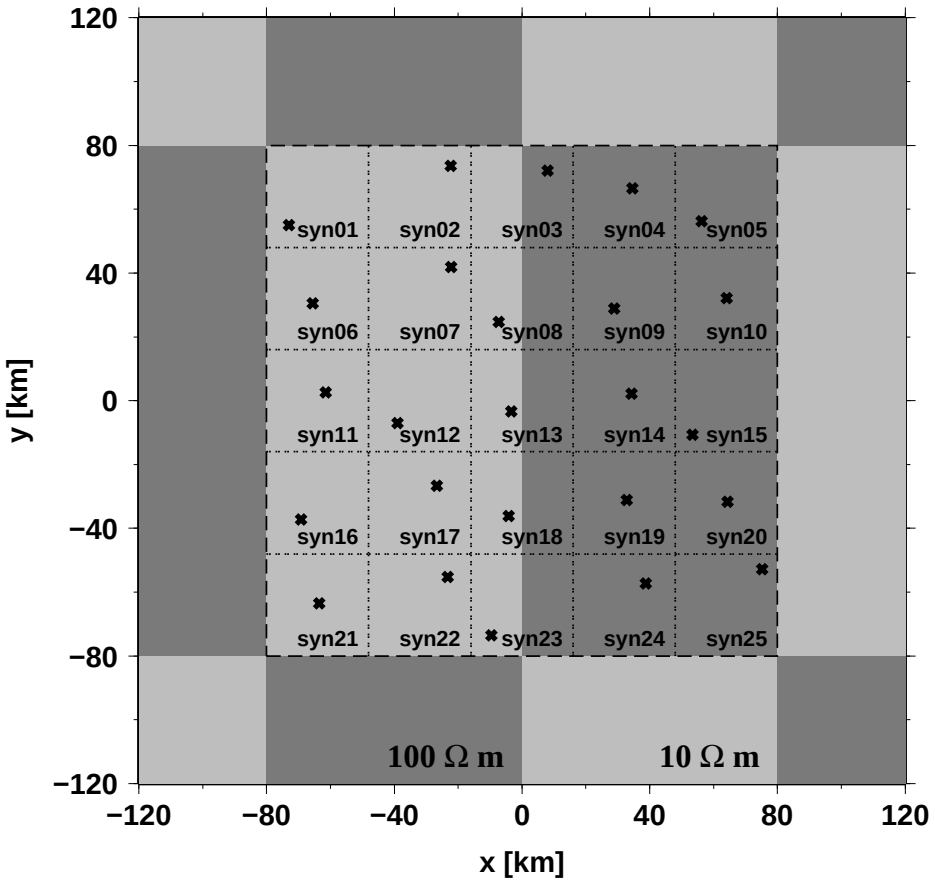

Figure S4. : Elongated checkerboard model used to demonstrate the effect of structure dimensionality on the distorted ssq impedance. The size of 10 and 100 Ohm-m anomalies in y-direction is twice of that in x-direction.

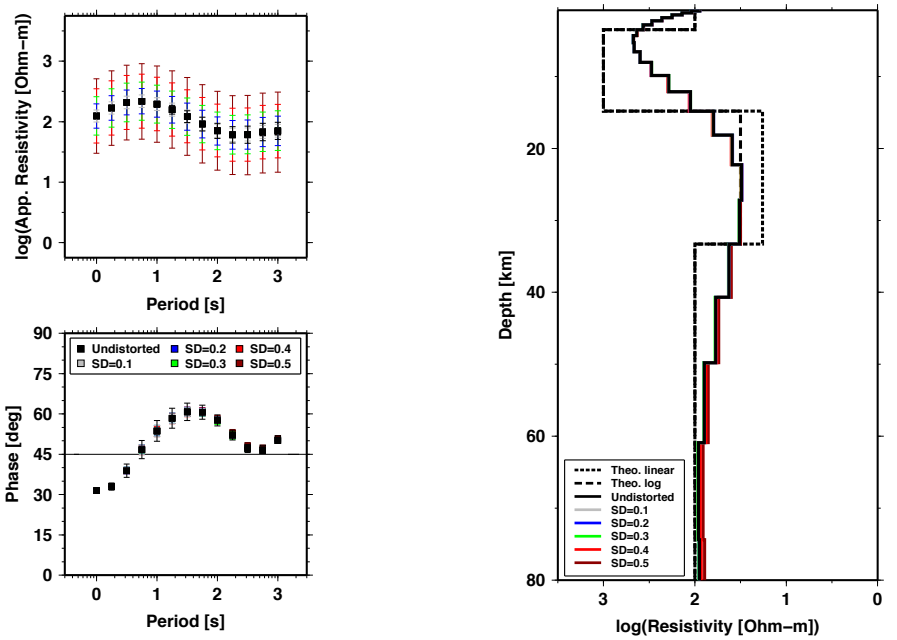

(a) (b)

Figure S5. : (a) Average ssq impedances of the MT responses from the elongated checkerboard (Figure S4) distorted with different galvanic distortion strengths. (b) The corresponding inverted 1D models (colored solid lines) and the theoretical models of the mean 1D profiles, $\sigma_{\mathrm{R}}(z)$, from this setting both in linear and logarithmic (Eqs. 3 and 4 in the main text) scaling (black dashed lines) and the 1D model from the undistorted data (black solid line) are shown for comparison.

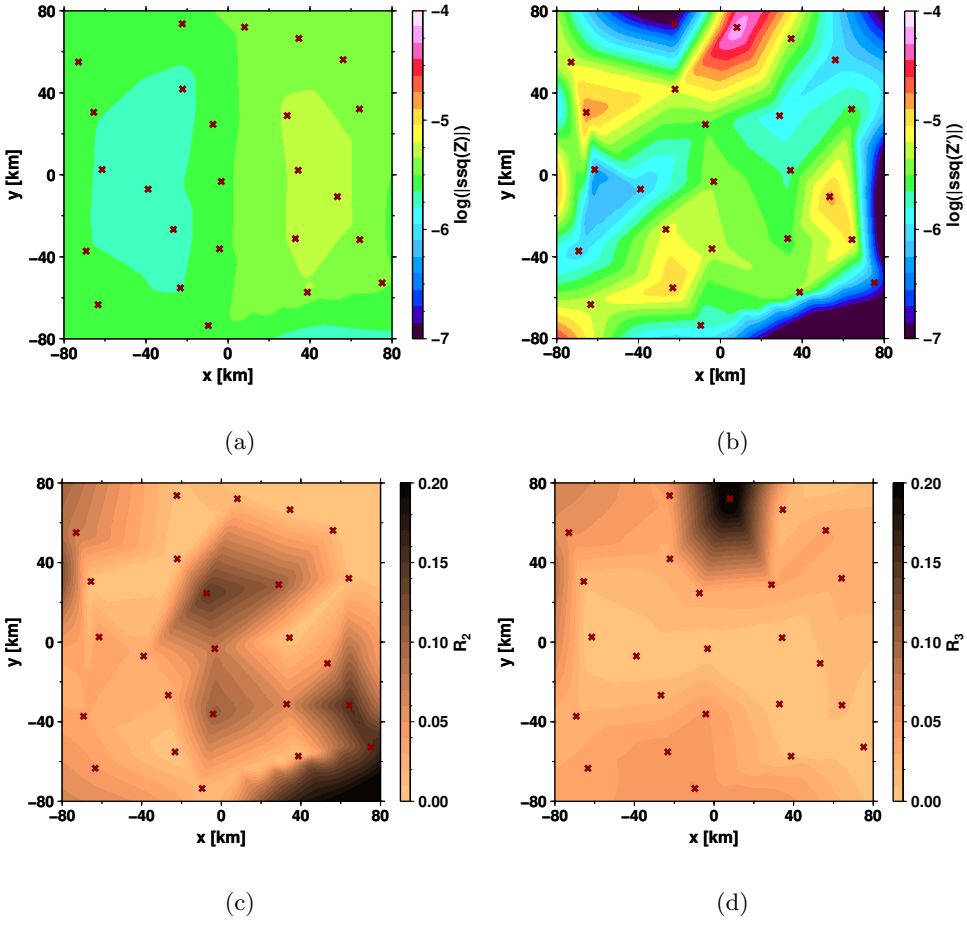

Figure S6. : Absolute values of the (a) undistorted and (b) distorted ssq rotational invariants, and the ratios R_2 and R_3 (Eqs. S5 and S6, respectively) at the period of 316.2 s calculated from the elongated checkerboard model (Figure S4).

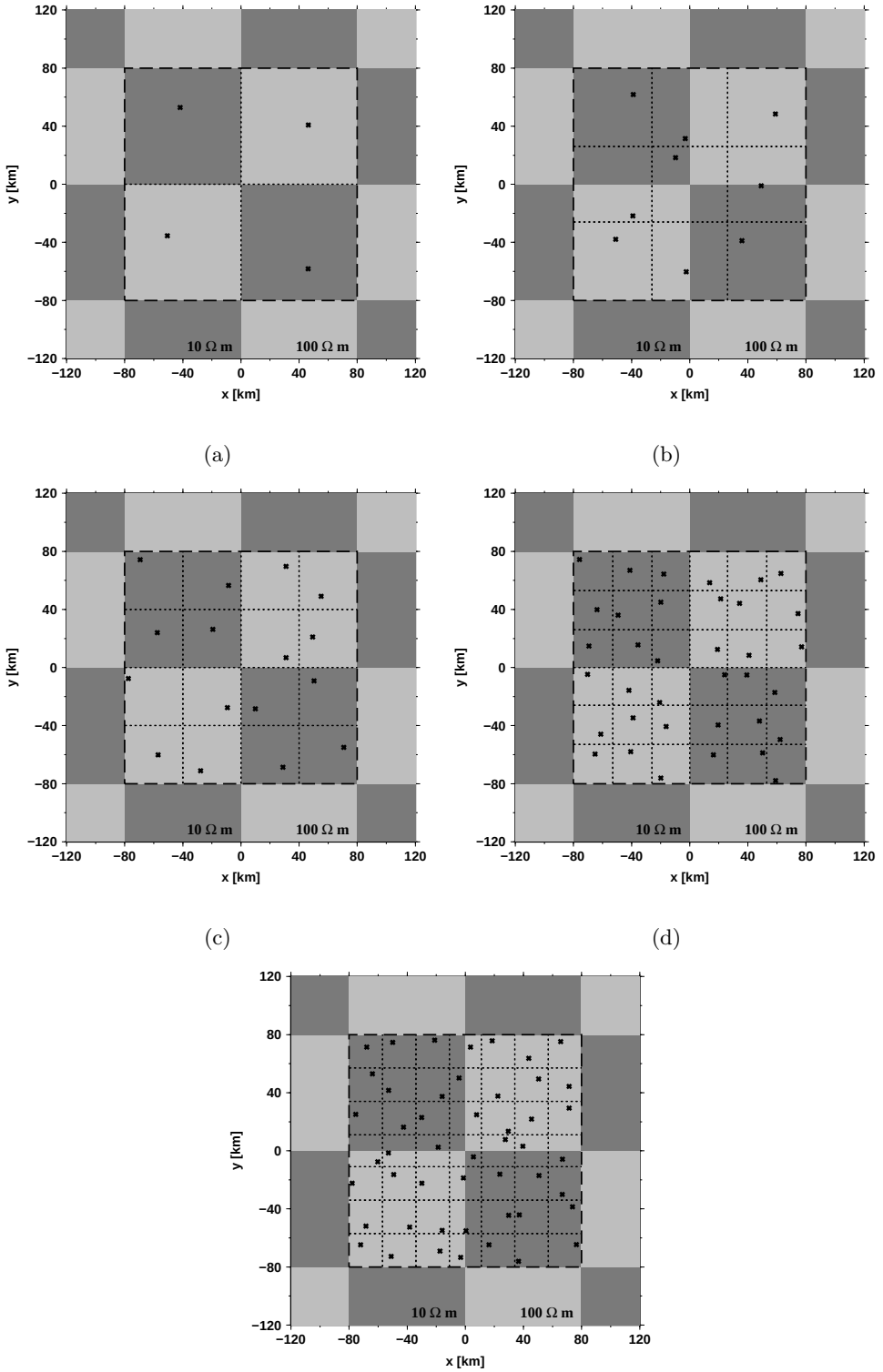

Figure S7. : The MT arrays with different number of stations—(a–e) 4, 9, 16, 36 and 49—for the calculation of the ratio $\bar{R}_1$ on the checkerboard model used in the main text.

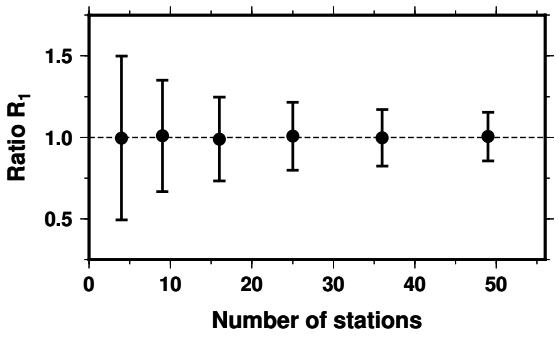

Figure S8. : The ratio $\bar{R}_1$ (Eq. S7) calculated from the MT arrays with different number of stations on the checkerboard model (Figure 8 in the main text) at the period of 316.2 s, where the error bar is the standard error of the ratio $\bar{R}_1$.

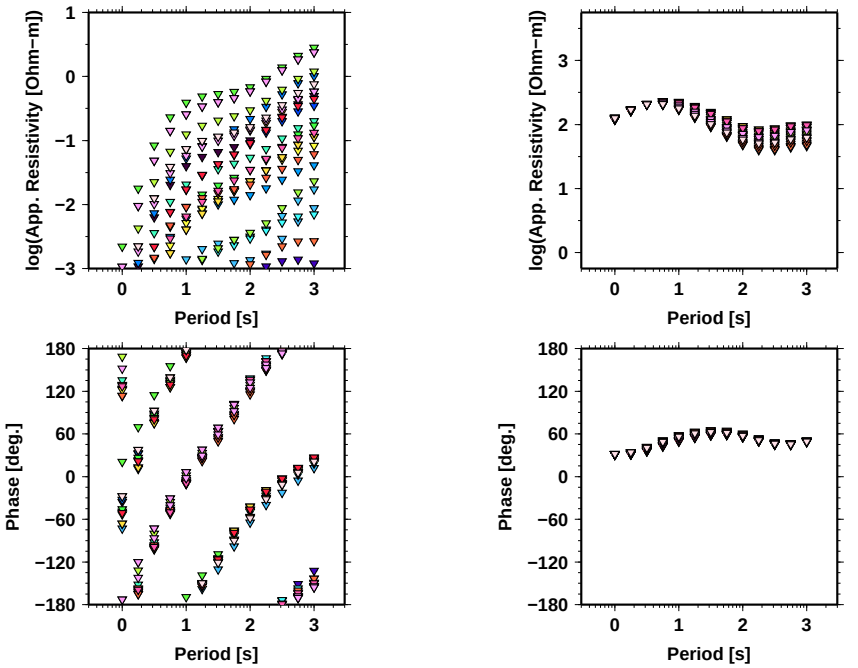

(a) xx

(b) xy

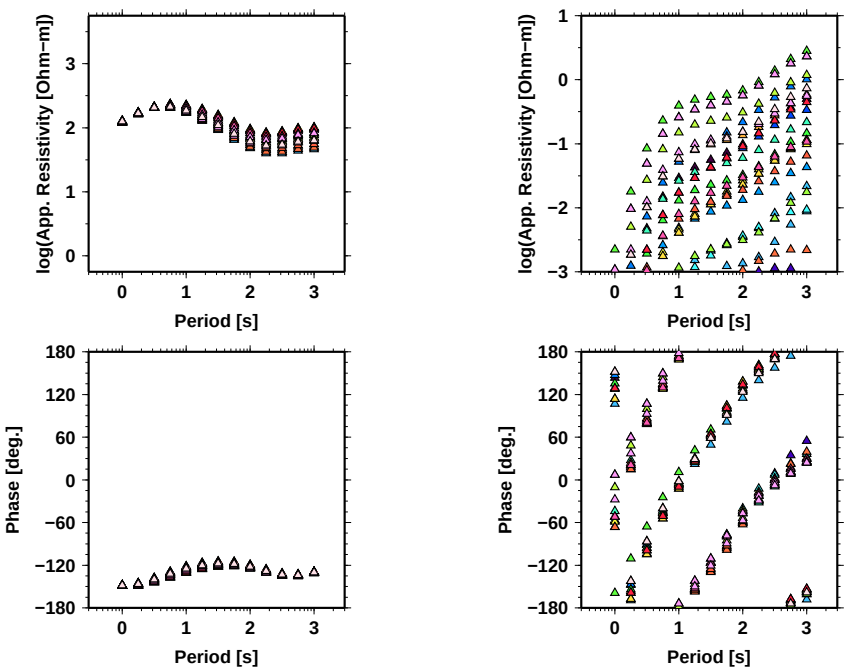

(c) yx

(d) yy

Figure S9. : Four components of MT impedances from the array of MT stations over the 3D anomalies (Figure 8 in the main text) without galvanic distortion. Each station is represented by a different symbol color.

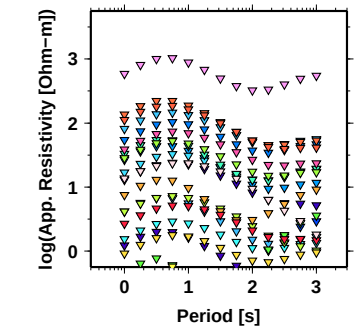

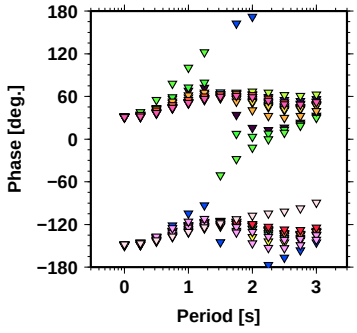

(a) xx

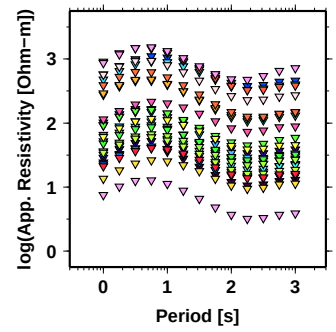

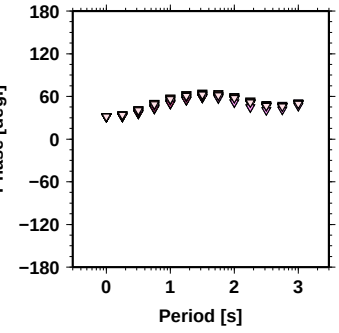

(b) xy

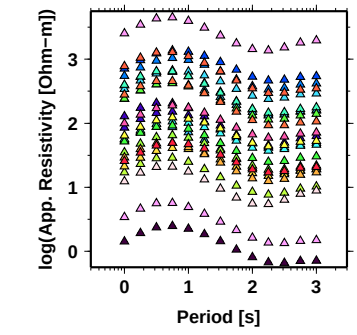

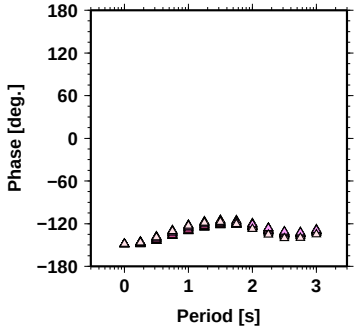

(c) yx

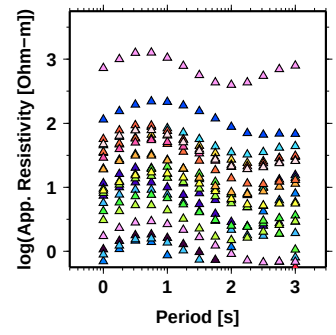

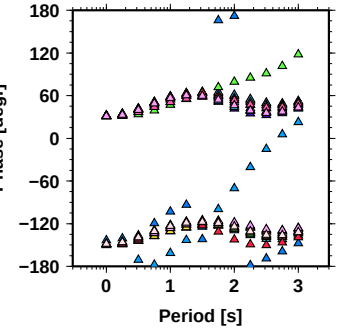

(d) yy

Figure S10. : Four components of MT impedances from the array of MT stations over the 3D anomalies (Figure 8 in the main text) with galvanic distortion. The set of distortion parameters (used in the main text) with an SD of 0.3 was applied. Each station is represented by a different symbol color.

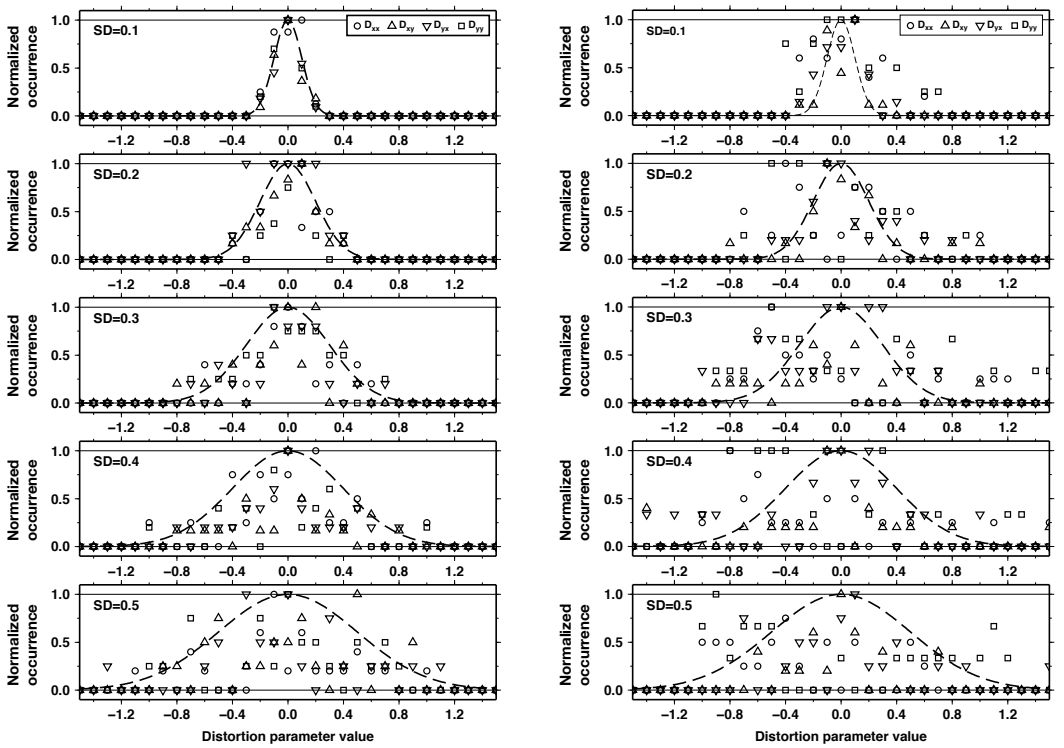

Figure S11. : (a) Distribution of random $(D_{xx}, D_{xy}, D_{yx}, D_{yy})$ cohorts with different SDs. The normalized occurrence is the number of occurrences divided by the maximum number of occurrence at a single parameter value. Each distribution is compared with the probability density function of the theoretical normal distribution for the given SD (dashed lines). (b) Distribution of random $(D_{xx}, D_{xy}, D_{yx}, D_{yy})$ cohorts derived from the Groom–Bailey cohorts (g, t, e, s) used in the main text.

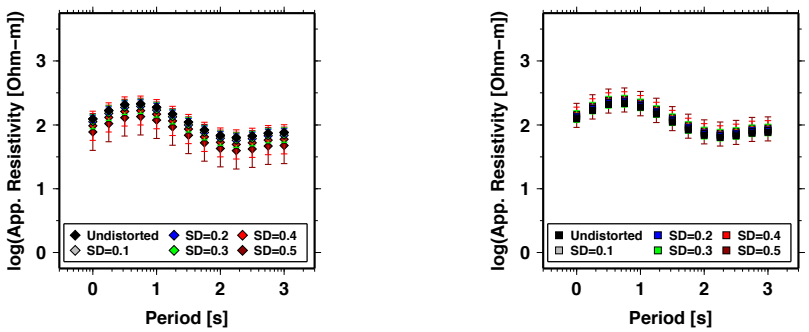

(a) (b)

Figure S12. : Average (a) det and (b) ssq impedances from the 1D datasets distorted with the PIM model at different galvanic distortion strengths.

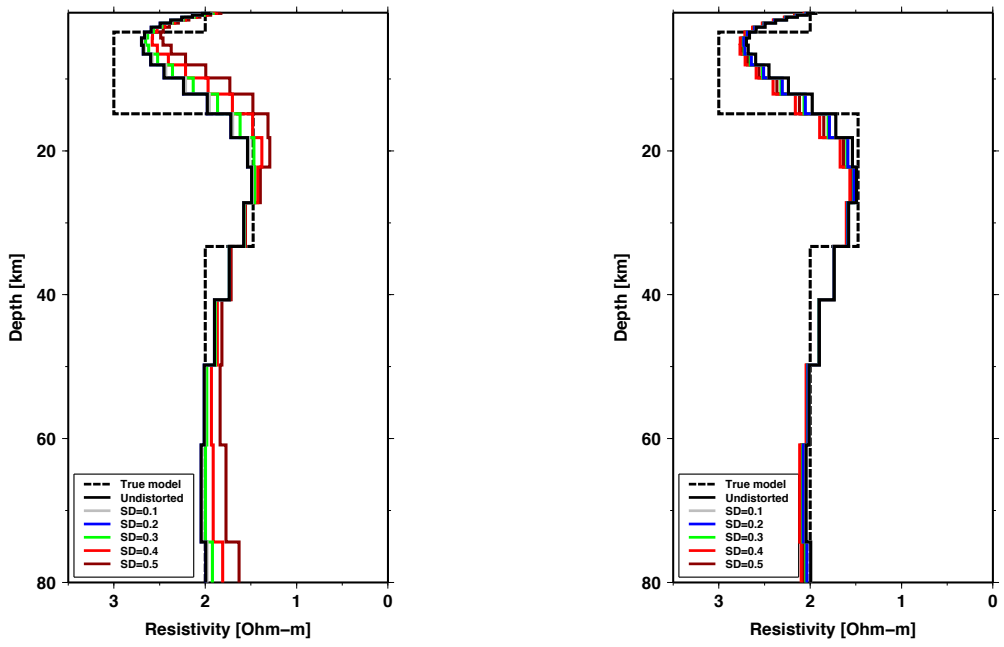

(a) (b)

Figure S13. : 1D models obtained by inverting the average (a) det and (b) ssq impedances from the 1D datasets distorted with the PIM model (Figure S12). The true structure (dashed lines) is also shown for comparison.

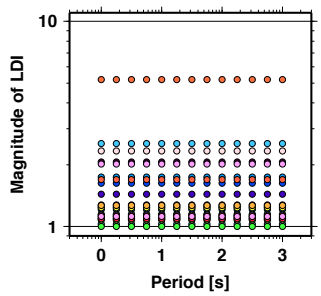

Figure S14. : LDIs from the distorted 1D data where a set of $(D_{xx}, D_{xy}, D_{yx}, D_{yy})$ cohorts with an SD of 0.5 was applied.

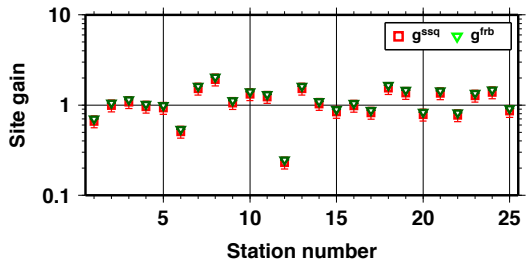

Figure S15. : Comparison of the Frobenius gains g_i^{frb} (triangles) with the mean apparent ssq gains g_i^{ssq} (squares) from the 1D example, where a set of $(D_{xx}, D_{xy}, D_{yx}, D_{yy})$ cohorts with an SD of 0.5 was applied.

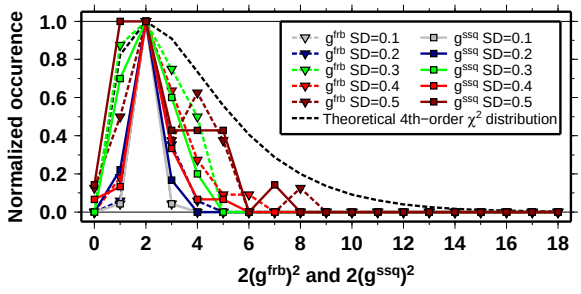

Figure S16. : Distribution of $2(g^{\mathrm{frb}})^2$ (dashed lines with symbols) derived from the random D_{ij} cohorts (Figure S11a) and that of $2(g^{\mathrm{ssq}})^2$ (solid lines with symbols) estimated from the distorted dataset. They are shown in comparison with the normalized theoretical χ^2 distribution of the fourth order (black dashed line).